Introduction to Precision Machine Design and Error Assessment

Chapter 8

The current issues in error modeling
3D volumetric positioning errors,

Edited by Samir Mekid,

Published by CRC Press, New York, NY, December 2008.

8 Current Issues in Error Modeling—3D Volumetric Positioning Errors

Charles Wang

CONTENTS

Machine tool accuracy is not linear. It is volumetric.

8.1 POSITIONING ERROR MODELING (SERIAL KINEMATICS MACHINES)

World competition requires good quality or accurate parts. Hence, the CNC machine tool positioning accuracy becomes very important. Twenty years ago, the largest machine tool positioning errors are leadscrew pitch error and thermal expansion error. Now, most of the above errors have been reduced by better leadscrew, linear encoder, and pitch error compensation. The largest machine tool positioning errors become squareness errors and straightness errors. Hence, to achieve higher 3D volumetric positioning accuracy, all three displacement errors, six straightness errors, and three squareness errors have to be measured. Using a conventional laser interferometer to measure these errors is rather difficult and costly. It usually takes days of machine downtime and experienced operator to perform these measurements. AQ1

It has been proposed to use the body diagonal displacement errors to define the volumetric positioning error [1]. However, the relations between the measured body diagonal displacement errors and the 21 rigid-body errors are not clear, and a more practical definition of a volumetric position error has been discussed but not defined yet. Hence, the current issues in machine errors modeling are to define and to determine the 3D volumetric positioning error of CNC machine tools. The definition should be directly linked to the 3D positioning errors and also practical to measure or determine such that it will be accepted by machine tool builders and used in the specification.

8.1.1 Rigid-Body Errors

In general, the errors should be a function of all three coordinates, x, y, and z. For serial kinematics machines, the x-, y-, and z-axes are orthogonal and stacking on each other. To simplify the theory, it is reasonable to assume the motions are rigid-body motions. Hence, the errors become functions of a single coordinate instead of three coordinates. In the following, the rigid-body errors are derived based on the rigid-body assumption; for each axis, there are three linear errors and six angular errors as shown in Figure 8.1. A three-axis machine, there are six errors per axis or a total of 18 errors plus three squareness errors as shown in Figure 8.2. These 21 rigid-body errors can be expressed as follows [2]:

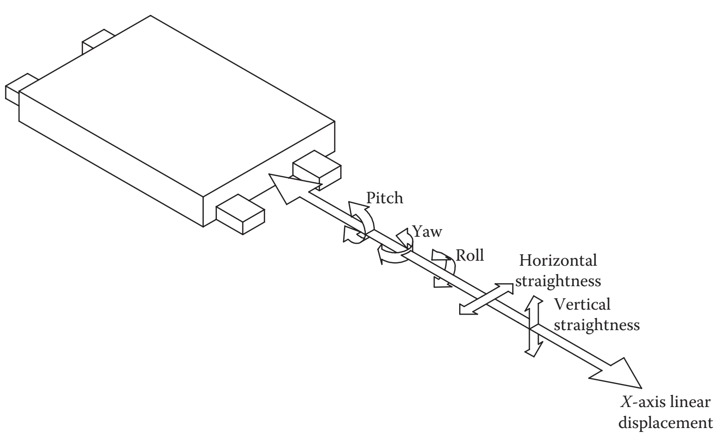

FIGURE 8.1 Linear and angular errors of a single axis.

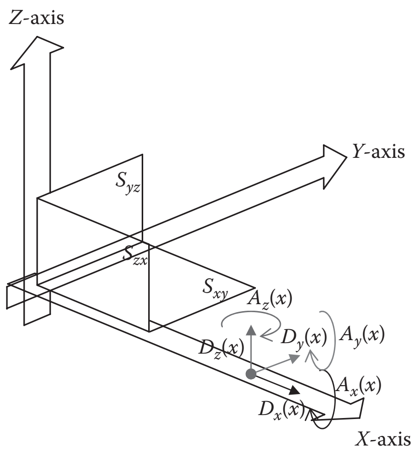

FIGURE 8.2 (See color insert following page XXX.) Squareness errors between axes.

Linear displacement errors: $D_x(x)$, $D_y(y)$, and $D_z(z)$
Vertical straightness errors: $D_y(x)$, $D_x(y)$, and $D_x(z)$
Horizontal straightness errors: $D_z(x)$, $D_z(y)$, and $D_y(z)$
Roll angular errors: $A_x(x)$, $A_y(y)$, and $A_z(z)$
Pitch angular errors: $A_y(x)$, $A_x(y)$, and $A_x(z)$
Yaw angular errors: $A_z(x)$, $A_z(y)$, and $A_y(z)$
Squareness errors: S_{xy}, S_{yz}, and S_{zx}

where D is the linear error, subscript is the error direction and the position coordinate is inside the parenthesis; A is the angular error, subscript is the axis of rotation and the position coordinate is inside the parenthesis.

Please note the positioning error caused by an angular error can be expressed as the Abbé offset times the angular errors. For example, positioning error in x-direction can be expressed as $zA_y(x) - y\,A_z(x)$, where z and y are the Abbé offset in the z- and y-directions, respectively.

8.1.2 Nonrigid-Body Errors

For nonrigid-body errors, they are also a function of the two other coordinate. To simplify the theory, assuming the variations is small and can be approximated by Taylor's expansion with the first-order term as the slope. The nonrigid-body errors become [3] AQ2

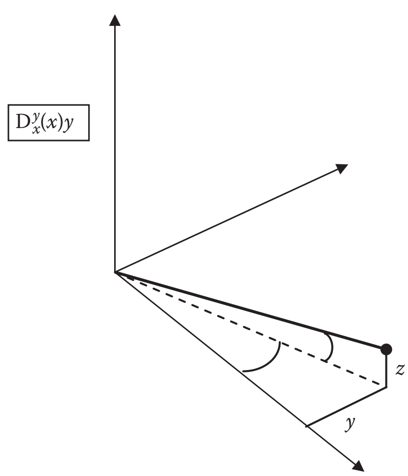

$$D_x(x)(y,\ z) = D_x(x) + D_x^y(x)y + D_x^z(x)z \tag{8.1}$$

$$D_y(x)(y,\ z) = D_y(x) + D_y^y(x)y + D_y^z(x)z \tag{8.2}$$

$$D_z(x)(y,\ z) = D_z(x) + D_z^y(x)y + D_z^z(x)z \tag{8.3}$$

$$D_x(y)(x,\ z) = D_x(y) + D_x^x(y)x + D_x^z(y)z \tag{8.4}$$

$$D_y(y)(x,\ z) = D_y(y) + D_y^x(y)x + D_y^z(y)z \tag{8.5}$$

$$D_z(y)(x,\ z) = D_z(y) + D_z^x(y)x + D_z^z(y)z \tag{8.6}$$

$$D_x(z)(x,\ y) = D_x(z) + D_x^x(z)x + D_x^y(z)y \tag{8.7}$$

$$D_y(z)(x,\ y) = D_y(z) + D_y^x(z)x + D_y^y(z)y \tag{8.8}$$

$$D_z(z)(x,\ y) = D_z(z) + D_z^x(z)x + D_z^y(z)y \tag{8.9}$$

Where D with a superscript is the slope and the superscript is the direction of the slope. There are a total of 27 parameters, 9 are the linear errors and 18 are the slopes of the nonrigid-body, that cause linear errors. AQ3

The angular errors are

$$A_x(x)(y,\ z) = A_x(x) + A_x^y(x)y + A_x^z(x)z \tag{8.10}$$

$$A_y(x)(y,\ z) = A_y(x) + A_y^y(x)y + A_y^z(x)z \tag{8.11}$$

$$A_z(x)(y,\ z) = A_z(x) + A_z^y(x)y + A_z^z(x)z \tag{8.12}$$

$$A_x(y)(x,\ z) = A_x(y) + A_x^x(y)x + A_x^z(y)z \tag{8.13}$$

$$A_y(y)(x,\ z) = A_y(y) + A_y^x(y)x + A_y^z(y)z \tag{8.14}$$

$$A_z(y)(x,\ z) = A_z(y) + A_z^x(y)x + A_z^z(y)z \tag{8.15}$$

$$A_x(z)(x,\ y) = A_x(z) + A_x^x(z)x + A_x^y(z)y \tag{8.16}$$

$$A_y(z)(x,\ y) = A_y(z) + A_y^x(z)x + A_y^y(z)y \tag{8.17}$$

$$A_z(z)(x,\ y) = A_z(z) + A_z^x(z)x + A_z^y(z)y \tag{8.18}$$

Where A with a superscript is the slope and the superscript is the direction of the slope. There are a total of 27 parameters: 9 are the angular errors and 18 are the slopes of the nonrigid-body caused angular errors.

For most machine tools, the structures are rather rigid. Hence, the nonrigid-body errors usually are small and negligible. However, for some large gantry type machines, because of the gravity and structure deformation, some nonrigid-body errors may not be negligible. The followings are two special cases as examples:

1. Horizontal milling machine of configuration *XFYZ* (see Section 8.1.3 for definition) with large counter weight along y-axis. All the slopes are negligible except the slopes in the y-direction.

$$D_x(x)(y,\ z) = D_x(x) + D_x^{\ y}(x)y \quad (8.19)$$

$$D_y(x)(y,z) = D_y(x) + D_y^{\ y}(x)y \quad (8.20)$$

$$D_z(x)(y,z) = D_z(x) + D_z^{\ y}(x)y \quad (8.21)$$

$$D_x(y)(x,z) = D_x(y) \quad (8.22)$$

$$D_y(y)(x,z) = D_y(y) \quad (8.23)$$

$$D_z(y)(x,z) = D_z(y) \quad (8.24)$$

$$D_x(z)(x,y) = D_x(z) \quad (8.25)$$

$$D_y(z)(x,y) = D_y(z) \quad (8.26)$$

$$D_z(z)(x,y) = D_z(z) \quad (8.27)$$

$$A_x(x)(y,z) = A_x(x) + A_x^{\ y}(x)y \quad (8.28)$$

$$A_y(x)(y,z) = A_y(x) + A_y^{\ y}(x)y \quad (8.29)$$

$$A_z(x)(y,z) = A_z(x) \quad (8.30)$$

$$A_x(y)(x,z) = A_x(y) \quad (8.31)$$

$$A_y(y)(x,z) = A_y(y) \quad (8.32)$$

$$A_z(y)(x,z) = A_z(y) \quad (8.33)$$

$$A_x(z)(x,y) = A_x(z) \quad (8.34)$$

$$A_y(z)(x,y) = A_y(z) \quad (8.35)$$

$$A_z(z)(x,y) = A_z(z) \quad (8.36)$$

There are five additional nonrigid-body errors. Here, for *XFYZ* configuration, the higher order nonrigid-body errors, $D_x^{\ y}(z)y$, $D_y^{\ y}(z)y$, $D_z^{\ y}(z)y$, $A_z^{\ y}(x)y$, $A_x^{\ y}(z)y$, $A_y^{\ y}(z)y$, and $A_y^{\ y}(z)y$, are negligible.

2. Large gantry vertical milling machine of configuration *XYFZ* and $X \gg Y, Z$. Here, the unbalanced weight shifting is along the *x*-direction. Hence, all the slopes are negligible except the slopes along the *x*-direction.

$$D_x(x)(y,z) = D_x(x) \quad (8.37)$$

$$D_y(x)(y,z) = D_y(x) \quad (8.38)$$

$$D_z(x)(y,z) = D_z(x) \quad (8.39)$$

$$D_x(y)(x,z) = D_x(y) + D_x^{\ x}(y)x \quad (8.40)$$

$$D_y(y)(x,z) = D_y(y) + D_y{}^x(y)x \tag{8.41}$$

$$D_z(y)(x,z) = D_z(y) + D_z{}^x(y)x \tag{8.42}$$

$$D_x(z)(x,y) = D_x(z) + D_x{}^x(z)x \tag{8.43}$$

$$D_y(z)(x,y) = D_y(z) + D_y{}^x(z)x \tag{8.44}$$

$$D_z(z)(x,y) = D_z(z) + D_z{}^x(z)x \tag{8.45}$$

$$A_x(x)(y,z) = A_x(x) \tag{8.46}$$

$$A_y(x)(y,z) = A_y(x) \tag{8.47}$$

$$A_z(x)(y,z) = A_z(x) \tag{8.48}$$

$$A_x(y)(x,z) = A_x(y) + A_x{}^x(y)x \tag{8.49}$$

$$A_y(y)(x,z) = A_y(y) + A_y{}^x(y)x \tag{8.50}$$

$$A_z(\mathrm{y})(x,z) = A_z(\mathrm{y}) \tag{8.51}$$

$$A_x(z)(x,y) = A_x(z) + A_x{}^x(z)x \tag{8.52}$$

$$A_y(z)(x,y) = A_y(z) + A_y{}^x(z)x \tag{8.53}$$

$$A_z(z)(x,y) = A_z(z). \tag{8.54}$$

There are 10 additional nonrigid-body errors. Here, the higher order nonrigid-body errors, $A_z{}^x(y)x$ and $A_z{}^x(z)x$, are negligible.

8.1.3 Machine Configurations and Positioning Errors

In most cases, coordinate measuring machines and machine tools can be classified into four configurations [4]. They are the *FXYZ*, *XFYZ*, *XYFZ*, and *XYZF* as shown in Figure 8.3a–d, respectively. Here, the axes before *F* show available motion directions of the workpiece with respect to the base, and the letters after *F* show the available motion directions of the tool (or probe) with respect to the base. For example, in *FXYZ*, the workpiece is fixed, and in *XYZF*, the tool is fixed.

8.1.3.1 Position Vector and Rotation Matrix

The vector positions of each stage, X, Y, and Z can be expressed as column vectors [2,4]:

$$X = \begin{bmatrix} x + D_x(x) \\ D_y(x) \\ D_z(x) \end{bmatrix} \tag{8.55}$$

$$Y = \begin{bmatrix} D_x(y) \\ y + D_y(y) \\ D_z(y) \end{bmatrix} \tag{8.56}$$

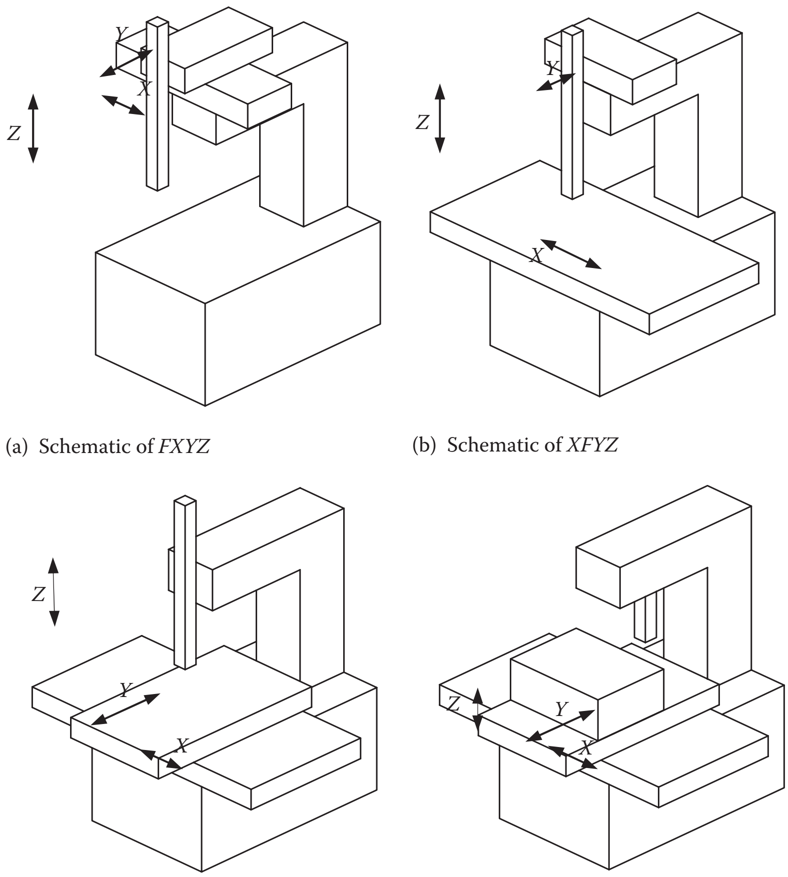

(a) Schematic of *FXYZ*

(b) Schematic of *XFYZ*

(c) Schematic of *XYFZ*

(d) Schematic of *XYZF*

FIGURE 8.3 Schematics of (a) *FXYZ*, (b) *XFYZ*, (c) *XYFZ*, and (d) *XYZF*.

$$X = \begin{bmatrix} D_x(z) \\ D_y(z) \\ z + D_z(z) \end{bmatrix} \tag{8.57}$$

To simplify the calculation, the squareness errors can be included in the straightness errors by defining the new straightness error as the sum of the old straightness errors and the squareness errors as shown:

$$D_x(y) = D_x(y)(\text{old}) + S_{xy} * y \tag{8.58}$$

$$D_x(z) = D_x(z)(\text{old}) + S_{zx} * z \tag{8.59}$$

$$D_y(z) = D_y(z)(\text{old}) + S_{yz} * z \tag{8.60}$$

The tool offset can be expressed as a column vector:

$$T = \begin{bmatrix} X_t \\ Y_t \\ Z_t \end{bmatrix} \tag{8.61}$$

where X_t, Y_t, and Z_t are the tool offset.

The rotation matrix can be expressed as

$$R(u) = \begin{bmatrix} 1 & A_z(u) & -A_y(u) \\ -A_z(u) & 1 & A_x(u) \\ A_y(u) & -A_x(u) & 1 \end{bmatrix} \tag{8.62}$$

where u = x, y, or z.

Please note $A_u(u)$ is much smaller than 1 and also an odd function of u; hence, $\mathbf{R}(u)\mathbf{U} = \mathbf{U}\mathbf{R}(u)$, and $\mathbf{R}(-u) = \mathbf{RI}(u)$, where $\mathbf{U}$ is a unit matrix and $\mathbf{RI}$ is the inverse matrix of $\mathbf{R}$.

8.1.3.2 Vectors and Rotation Matrices Calculation

If the positions of the X, Y, and Z stages are represented by the vectors $\mathbf{X}$, $\mathbf{Y}$, and $\mathbf{Z}$, respectively. The angular errors of the X, Y, and Z stages are represented by the rotation matrices $\mathbf{R}(x)$, $\mathbf{R}(y)$, and $\mathbf{R}(z)$. The offset of the tool tip (or probe) are represented by the vector $\mathbf{T}(X_t, Y_t, Z_t)$. The actual positions with respect to the workpiece or machine coordinate can be represented by the vector $\mathbf{P}$. As shown in Ref. [5], the actual position vector $\mathbf{P}$ for the four configurations can be expressed in a machine coordinate as the followings [4]:

$$\text{For } FXYZ,\ \mathbf{P} = X + \mathbf{RI}(x)\mathbf{Y} + \mathbf{RI}(x)\mathbf{RI}(y)\mathbf{Z} + \mathbf{RI}(x)\mathbf{RI}(y)\mathbf{RI}(z)\mathbf{T} \tag{8.63}$$

$$\text{For } XFYZ, \mathbf{P} = \mathbf{RI}(x)\mathbf{X} + \mathbf{RI}(x)\mathbf{Y} + \mathbf{RI}(x)\mathbf{RI}(y)\mathbf{Z} + \mathbf{RI}(x)\mathbf{RI}(y)\mathbf{RI}(z)\mathbf{T} \tag{8.64}$$

$$\text{For } XYFZ, \mathbf{P} = \mathbf{RI}(y)\mathbf{RI}(x)\mathbf{X} + \mathbf{RI}(y)\mathbf{Y} + \mathbf{RI}(y)\mathbf{RI}(x)\mathbf{Z} + \mathbf{RI}(x)\mathbf{RI}(y)\mathbf{RI}(z)\mathbf{T} \tag{8.65}$$

$$\text{For } XYZF, \mathbf{P} = \mathbf{RI}(z)\mathbf{RI}(y)\mathbf{RI}(x)X + \mathbf{RI}(z)\mathbf{RI}(y)\mathbf{Y} + \mathbf{RI}(z)\mathbf{Z} + \mathbf{RI}(x)\mathbf{RI}(y)\mathbf{RI}(z)\mathbf{T} \tag{8.66}$$

The actual tool tip position can be expressed as a column vector:

$$P = \begin{bmatrix} P_x \\ P_y \\ P_z \end{bmatrix} \tag{8.67}$$

8.1.3.3 Positioning Errors in Four Configurations

Substitute the position vectors, Equations 8.55 through 8.57, and Equations 8.61 and 8.62 into the above equations, we obtained the actual tool tip position, Equation 8.67 in the followings [5,6].

For $FXYZ$ configuration, Equation 8.63 becomes

$$P_x - x = [D_x(x) - y * A_z(x) + z * A_y(x)] + [D_x(y) + z * Ay(y)] + [D_x(z)] \tag{8.68}$$

$$P_y - y = [D_y(x) - z * A_x(x)] + [D_y(y) - z * A_x(y)] + [D_y(z)] \tag{8.69}$$

$$P_z - z = [D_z(x) + y * A_x(x)] + [D_z(y)] + [D_z(z)]. \tag{8.70}$$

where P_x–x, P_y–y, and P_z–z are the positioning errors in the x-, y-, and z-directions, respectively. Additional errors caused by a tool offset of X_t, Y_t, and Z_t are

$$P_{tx} = X_t + [-Y_t * A_z(x) + Z_t * A_y(x)] + [-Y_t * A_z(y) + Z_t * A_y(y)] + [-Y_t * A_z(z) + Z_t * A_y(z)] \tag{8.71}$$

$$P_{ty} = Y_t + [X_t * A_z(x) - Z_t * A_x(x)] + [X_t * A_z(y) - Z_t * A_x(y)] + [X_t * A_z(z) - Z_t * A_x(z)] \tag{8.72}$$

$$P_{tz} = Z_t + [-X_t * A_y(x) + Y_t * A_x(x)] + [-X_t * A_y(y) + Y_t * A_x(y)] + [-X_t * A_y(z) + Y_t * A_x(z)] \quad (8.73)$$

Similarly, for *XFYZ* configuration, Equation 8.64 becomes

$$P_x - x = [D_x(x) - y * A_z(x) + z * A_y(x)] + [D_x(y) + z * A_y(y)] + [D_x(z)] \quad (8.74)$$ AQ4

$$P_y - y = [D_y(x) + x * A_z(x) - z * A_x(x)] + [D_y(y) - z * A_x(y)] + [D_y(z)] \quad (8.75)$$

$$P_z - z = [D_z(x) - x * A_y(x) + y * A_x(x)] + [D_z(y)] + [D_z(z)]. \quad (8.76)$$

The errors caused by a tool offset are the same as in *FXYZ*, Equations 8.71 through 8.73 AQ5

Similarly, for *XYFZ* configuration, Equation 8.65 becomes

$$P_x - x = [D_x(x) + z * A_y(x)] + [D_x(y) - y * A_z(y) + z * A_y(y)] + [D_x(z)] \quad (8.77)$$

$$P_y - y = [D_y(x) + x * A_z(x) - z * A_x(x)] + [D_y(y) + x * A_z(y) - z * A_x(y)] + [D_y(z)] \quad (8.78)$$

$$P_z - z = [D_z(x) - x * A_y(x)] + [D_z(y) - x * A_y(y) + y * A_x(y)] + [D_z(z)]. \quad (8.79)$$

The errors caused by a tool offset are the same as in *FXYZ*, Equations 8.71 through 8.73.

Finally for *XYZF* configuration, Equation 8.66 becomes,

$$P_x - x = [D_x(x)] + [D_x(y) - y * A_z(y)] + [D_x(z) - y * A_z(z) + z * A_y(z)] \quad (8.80)$$

$$P_y - y = [D_y(x) + x * A_z(x)] + [D_y(y) + x * A_z(y)] + [D_y(z) + x * A_z(z) - zA_x(z)] \quad (8.81)$$

$$P_z - z = [D_z(x) - x * A_y(x)] + [D_z(y) - x * A_y(y) + y * A_x(y)] + [D_z(z) - x * A_y(z) + y * A_x(z)]. \quad (8.82)$$

The above results can also be derived by the Stacking model and Abbé offset. The displacement errors caused by the pitch, yaw and roll angular errors are the Abbé offset times the angular errors. The sign is determined by the right-hand rule.

For the configuration *FXYZ*, x-axis is mounted on a fixed base, y-axis is mounted on the x-axis, and z-axis is mounted on the y-axis. Hence, for x-axis movement, there is no Abbé offset on x and the angular error terms are $y^*A_x(x)$, $y^*A_z(x)$, $-z^*A_x(x)$, and $z^*A_y(x)$; for y-axis movement, there are no Abbé offset on x and y and the angular error terms are $-z^*A_x(y)$ and $z^*A_y(y)$; for z-axis movement, there are no Abbé offsets on x, y, and z and there is no angular error term. The results are the same as Equations 8.68 through 8.70.

Similarly, for the configuration *XFYZ*, x-axis is mounted on a fixed base, y-axis is mounted on the x-axis, and z-axis is mounted on the y-axis. Hence, for x-axis movement, there are all three Abbé offsets and the angular error terms are $-x^*A_y(x)$, $x^*A_z(x)$, $y^*A_x(x)$, $-y^*A_z(x)$, $-z^*A_x(x)$, and $z^*A_y(x)$; for y-axis movement, there are no Abbé offsets on x and y and the angular error terms are $-z^*A_x(y)$ and $z^*A_y(y)$; for z-axis movement, there are no Abbé offsets on x, y, and z and there is no angular error term. The results are the same as Equations 8.74 through 8.76.

Similarly, for the configuration *XYFZ*, x-axis is mounted on a fixed base, y-axis is mounted on the x-axis, and z-axis is mounted on a fixed base. Hence, for x-axis movement, there is no Abbé offset on y and the angular error terms are $-x^*A_y(x)$, $x^*A_z(x)$, $-z^*A_x(x)$, and $z^*A_y(x)$; for y-axis movement, there are all three Abbé offsets, and the angular terms are $x^*A_y(y)$, $x^*A_z(y)$, $y^*A_x(y)$, $-y^*A_z(y)$, $-z^*A_x(y)$, and $z^*A_y(y)$; for z-axis movement, there is no Abbé offset on x, y, and z and no angular term. The results are the same as Equations 8.77 through 8.79.

Finally for the configuration *XYZF*, x-axis is mounted on a fixed base, y-axis is mounted on the x-axis, and z-axis is mounted on the y-axis and the spindle is fixed. Hence, for x-axis movement, there are no Abbé offsets on x and y and the angular error terms are $-z^*A_x(x)$ and $z^*A_y(x)$; for y-axis movement, there is no Abbé offset on z, and the angular error terms are $-x^*A_y(y)$, $x^*A_z(y)$, $y^*A_x(y)$, $-y^*A_z(y)$; for z-axis movement, there are all three Abbé offsets and the angular error terms are $-x^*A_y(z)$, $x^*A_z(z)$, $y^*A_x(z)$, $-y^*A_z(z)$, $-z^*A_x(z)$ and $z^*A_y(z)$. The results are the same as Equations 8.80 through 8.82.

8.2 POSITIONING ERROR COMPENSATION MODELING

The sum of all errors in the x-, y-, and z-directions are E_x, E_y, and E_z, respectively.

$$\begin{aligned} E_x(x,y,z) = {} & D_x(x)+D_x(y)+D_x(z)+D_x^x(y)x-(z+Z_t)*A_y(x)+Y_t*A \\ & -(z+Z_t)*[A_y(y)+A_y^x(y)x]+Y_t*A_z(y)-Z_t*A_y(z)+Y_t*A_z(z) \end{aligned} \tag{8.83}$$

$$\begin{aligned} E_y(x,y,z) = {} & D_y(y)+D_y^x(y)x+D_y(z)+D_y(x)-(x+X_t)*A_z(y)+(z+Z_t) \\ & *[A_x(y)+A_x^x(y)x]-X_t*A_z(z)+Z_t*A_x(z)-X_t*A_z(x)+(z+Z_t)*A_x(x) \end{aligned} \tag{8.84}$$

$$\begin{aligned} E_z(x,y,z) = {} & D_z(z)+D_z(x)+D_z(y)+D_z^x(y)x-Y_t*A_x(z)+X_t*A_y(z)-Y_t \\ & *A_x(x)+X_t*A_y(x)-Y_t*[A_x(y)+A_x^x(y)x]+(x+X_t)*[A_y(y)+A_y^x(y)x] \end{aligned} \tag{8.85}$$

For the case the reference point is the tool tip, then $X_t = Y_t = Z_t = 0$. Hence, the sums of errors, Equations 8.83 through 8.85, reduce to the followings:

$$E_x(x,y,z) = D_x(x)+D_x(y)+D_x(z)+D_x^{\ x}(y)x-z*A_y(x)-z*[A_y(y)+A_y^{\ x}(y)x] \tag{8.86}$$

$$E_y(x,y,z) = D_y(y)+D_y^{\ x}(y)x+D_y(z)+D_y(x)-x*A_z(y)+z*[A_x(y)+A_x^{\ x}(y)x]+z*A_x(x) \tag{8.87}$$

$$E_z(x,y,z) = D_z(z)+D_z(x)+D_z(y)+D_z^{\ x}(y)x+A_x^{\ x}(y)x+x*[A_y(y)+A_y^{\ x}(y)x] \tag{8.88}$$

8.2.1 Displacement Error Compensation

Most machine controllers can provide compensation for repeatable leadscrew or encoder errors on each axis of motion. Usually this is called pitch error compensation.

The errors in the x-, y- and z-directions can be expressed as

$$E_x(x) = D_x(x) \tag{8.89}$$

$$E_y(y) = D_y(y) \tag{8.90}$$

$$E_z(z) = D_z(z) \tag{8.91}$$

8.2.2 Squareness and Straightness Error Compensation

Many machines with advanced controllers can provide compensation for repeatable displacement errors (leadscrew or encoder errors), vertical and horizontal straightness errors (guide way flatness error), and squareness errors. The errors in the x-, y-, and z-directions can be expressed as

$$E_x(x,y,z) = D_x(x)+D_x(y)+D_x(z) \tag{8.92}$$

$$E_y(x,y,z) = D_y(x)+D_y(y)+D_y(z) \tag{8.93}$$

$$E_z(x,y,z) = D_z(x)+D_z(y)+D_z(z) \tag{8.94}$$

8.2.3 Angular Error Compensation

Most machine controllers do not have the capability of compensate angular error and usually the angular error times the Abbé offset is included in the measured straightness errors. However, many times the tool offsets and the effect of angular errors are different. The errors in the x-, y-, and z-directions can be expressed as

$$\begin{aligned} E_x(x,y,z) &= D_x(x)+D_x(y)+D_x(z)+(z+Z_t)*A_y(x)+Y_t*A_z(x) \\ &\quad -(z+Z_t)*A_y(y)+Y_t*A_z(y)-Z_t*A_y(z)+Y_t*A_z(z) \end{aligned} \tag{8.95}$$

$$\begin{aligned} E_y(x,y,z) &= D_y(x)+D_y(y)+D_y(z)-(\mathrm{x}+X_t)*A_z(y)+(z+Z_t)*A_x(y) \\ &\quad -X_t*A_z(z)+Z_t*A_x(z)-X_t*A_z(x)+(z+Z_t)*A_x(x) \end{aligned} \tag{8.96}$$

$$\begin{aligned} E_z(x,y,z) &= D_z(x)+D_z(y)+D_z(z)+D_z^{\;x}(y)x-Y_t*A_x(z)+X_t*A_y(z) \\ &\quad -Y_t*A_x(x)+X_t*A_y(x)-Y_t*A_x(y)+(x+X_t)*A_y(y) \end{aligned} \tag{8.97}$$

8.2.4 Nonrigid-Body Error Compensation

Same as the angular error compensation, the nonrigid-body errors such as weight shift errors and counter weight errors are included in the measured straightness errors. The errors in the x-, y-, and z-directions can be expressed as

$$\begin{aligned} E_x(x,y,z) &= D_x(x)+D_x(y)+D_x(z)+D_x^x(y)x-(z+Z_t)*A_y(x)+Y_t*A_z(x) \\ &\quad -(z+Z_t)*[A_y(y)+A_y^x(y)x]+Y_t*A_z(y)-Z_t*A_y(z)+Y_t*A_z(z) \end{aligned} \tag{8.98}$$

$$\begin{aligned} E_y(x,y,z) &= D_y(y)+D_y^x(y)x+D_y(z)+D_y(x)-(x+X_t)*A_z(y)+(z+Z_t) \\ &\quad *[A_x(y)+A_x^x(y)x]-X_t*A_z(z)+Z_t*A_x(z)-X_t*A_z(x)+(z+Z_t)*A_x(x) \end{aligned} \tag{8.99}$$

$$\begin{aligned} E_z(x,y,z) &= D_z(z)+D_z(x)+D_z(y)+D_z^x(y)x-Y_t*A_x(z)+X_t*A_y(z)-Y_t*A_x(x) \\ &\quad +X_t*A_y(x)-Y_t*[A_x(y)+A_x^x(y)x]+(x+X_t)*[A_y(y)+A_y^x(y)x] \end{aligned} \tag{8.100}$$

8.2.5 3D Grid Point Error Compensation

In many advanced controllers, the nonrigid-body repeatable errors can be compensated by a 3D grid point error map. In such 3D error compensation, the error compensation for an arbitrary interior point P, shown in Figure 8.4, is interpolated by the surrounding eight error compensation grid points.

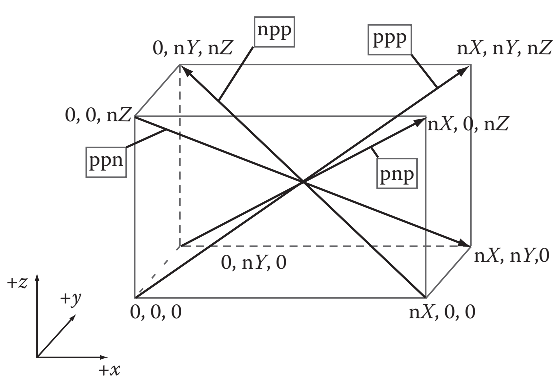

FIGURE 8.4 (See color insert following page XXX.) Four body diagonal directions.

The error values of these 8 grid points are measured and input to the control. The following equation is used to calculate the error compensation [7]:

For error compensation in x-axis direction for point P

$$\begin{aligned} Cx = {} & C1x\cdot(1-x)(1-y)(1-z)+C2x\cdot x(1-y)(1-z) \\ & +C3x\cdot xy(1-z)+C4x\cdot(1-x)y(1-z) \\ & +C5x\cdot(1-x)(1-y)z+C6x\cdot x(1-y)z \\ & +C7x\cdot xyz+C8x\cdot(1-x)yz \end{aligned} \tag{8.101}$$

AQ6

Where, Cnx is the measured error value for X-axis at grid points (n = 1, 2,…, 8)

$$x=\frac{|Px-P1x|}{|P2x-P1x|} \tag{8.102}$$

$$y=\frac{|Py-P1y|}{|P2y-P1y|} \tag{8.103}$$

$$z=\frac{|Pz-P1z|}{|P2z-P1z|} \tag{8.104}$$

Error calculation (Equation 8.101 reflects the influence the surrounding grid points. Similarly, for error compensation in y- and z-directions, the interpolation formulae are the same but errors are in y- and z-directions.

8.2.6 Thermal Expansion and Distortion Compensation

The thermal behavior of a machine tool is one of the major factors influencing the final workpiece accuracy. In relation with the currently increasing power output of the machine spindles and the rising dynamics of all driven movements, the influence of the machine thermal state is continuously rising. The prediction of thermal deformations is hardly executable in the design phase of a new machine tool model. Theoretical work in the field of modeling of temperature distribution within the machine frame has not been satisfactory concluded [8].

The causes of thermal deviations may be divided into two basic categories. The first part is from the thermal loadings resulting from the machine tool operation. The most significant sources of heat in a CNC machine tool are the spindle, ballscrew alternatively linear motor, and heat coming from the cutting process. The second part is represented by deviations raised from the thermal deformations of the machine frame caused by external influences—mainly the environmental temperature in the shop floor, temperature variations, airflow, direct sunshine, etc.

Currently machine tool builders are striving to increase machine tool accuracy and productivity by applying various methods covering machine frame design optimization, assembly work improvement, introduction of several cooling systems, etc. To further improve the machine positioning accuracy, an intelligent controller can be used to compensate these errors, provided that the 3D volumetric positioning errors and the machine temperature distributions can be measured. Furthermore, the measurement has to be performed in a short time such that the machine thermal state remains constant.

In a real machine shop environment, under various spindle loads and feed rates, the machine thermal expansion may cause large 3D volumetric positioning errors. Using the measured position errors, several error maps could be generated. Compensation tables at an actual thermal state can be interpolated to achieve higher accuracy at various thermal loadings.

Since the 3D volumetric position errors $E_x(x, y, z)$, $E_y(x, y, z)$, and $E_z(s, y, z)$ can be measured by the laser vector technique (see Section 3.2.2) in less than 1 h, we can assume the machine temperature is constant during the measurement. The measured position errors at two different temperatures, T_m and T_n, can be expressed as $E_x(x, y, z, T_m)$, $E_y(x, y, z, T_m)$, and $E_z(x, y, z, T_m)$, and $E_x(x, y, z, T_n)$, $E_y(x, y, z, T_n)$, and $E_z(x, y, z, T_n)$. Assuming the machine errors are linear between T_m and T_n, for a temperature T_u, where $T_m > T_u > T_n$, the position errors at T_u can be interpolated as the follows:

$$E_x\left(x,y,z,T_u\right)=[E_x(x,y,z,T_m)-E_x(x,y,z,T_n)]*(T_u-T_n)/(T_m-T_n)+E_x(x,y,z,T_n) \quad (8.105)$$

$$E_y(x,y,z,T_u)=[E_y(x,y,z,T_m)-E_y(x,y,z,T_n)]*(T_u-T_n)/(T_m-T_n)+E_y(x,y,z,T_n) \quad (8.106)$$

$$E_z(x,y,z,\mathrm{T_u})=[E_z(x,y,z,T_m)-E_z(x,y,z,T_n)]*(\mathrm{Tu}-T_n)/(T_m-T_n)+E_z(x,y,z,T_w) \quad (8.107)$$

To cover a large operational temperature range, we may need to measure the errors at several thermal states.

To demonstrate this, considerable work has been performed by Svoboda et al. [8,9] by measuring the 3D volumetric positioning errors and machine temperature distributions at various spindle rpm, feed rates, and ambient temperatures in a machining center of *XYFZ* configuration as shown in Figure 8.5. Some of the results are shown below. AQ7

8.2.7 Temperature History

The temperature data is displayed in Figure 8.6 for the sensor located on the spindle, z-column, x-middle, and y-front at six measurement runs. It is clear that the main heating occurs in parts close to the spindle. The temperatures were continuously increased due to the spindle heating and rapid xyz-axes motion. These temperature changes caused different thermal deformations of the z-column, and the xy-bed yielding into the measured variations of the 3D volumetric positioning accuracy.

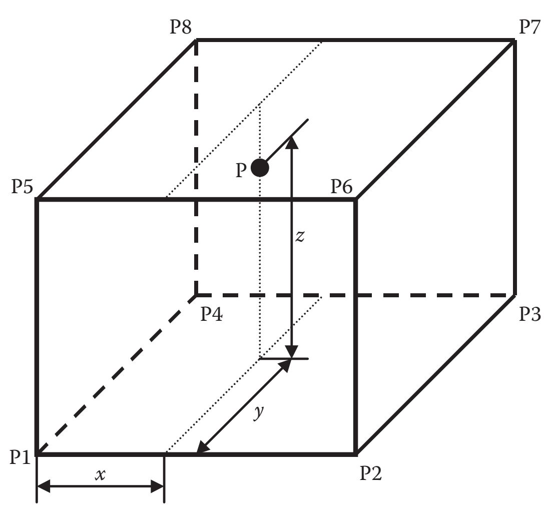

FIGURE 8.5 Schematic drawing showing the 3D grid point P.

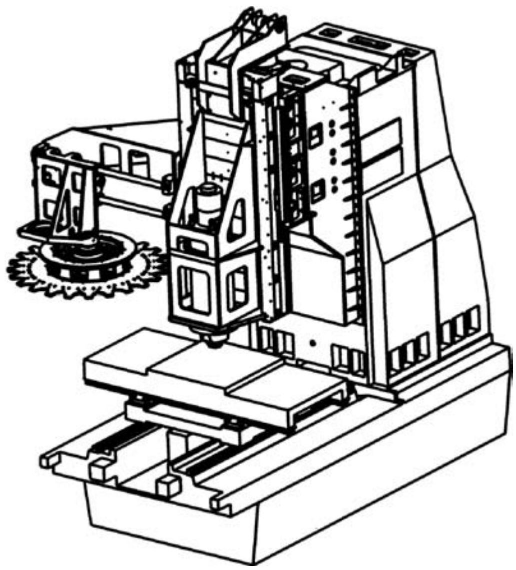

FIGURE 8.6 A schematic drawing of the vertical machining center MCFV5050LN.

8.2.8 Straightness Errors

Straightness errors were measured for all x-, y-, and z-axes and the changes were relatively small over the temperature range. Figure 8.7 shows the x-axis straightness errors $D_y(x)$ under various thermal states Run #1 to Run #6. The maximums varied between −0.010 and −0.007 mm. Figure 8.8 shows the y-axis straightness errors $D_x(y)$ under the same various thermal states. The maximums varied between −0.012 and −0.003 mm. Figure 8.9 shows the z-axis straightness errors $D_x(z)$ under the same various thermal states. The maximums varied between 0.009 and 0.003 mm. Figure 8.10 shown the z-axis straightness errors $D_y(z)$ under the same various thermal states. The maximums varied between 0.017 and 0.013 mm.

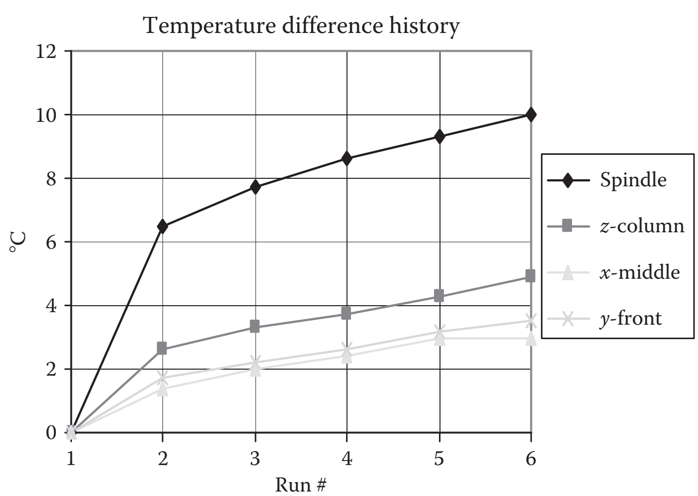

FIGURE 8.7 Measured temperature history at four locations.

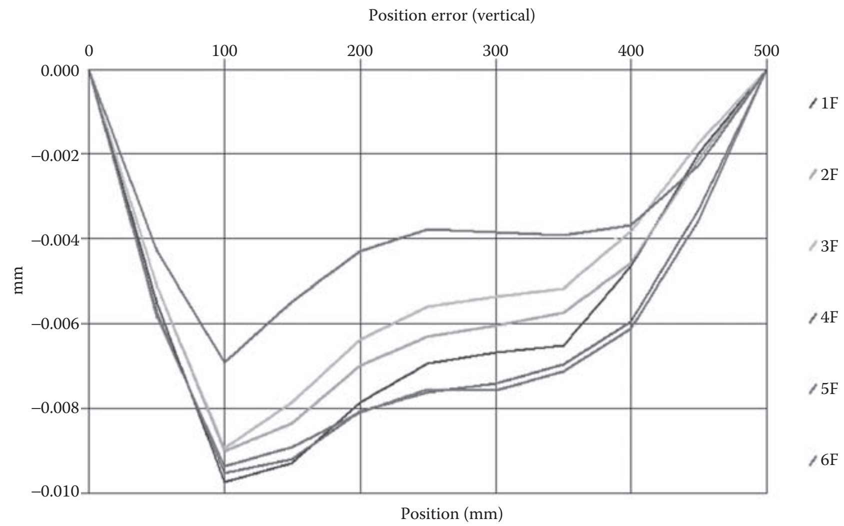

FIGURE 8.8 (See color insert following page XXX.) Measured *x*-axis straightness errors *Dy*(*x*) at six different thermal conditions, Run # 1 to Run #6.

8.2.9 Temperature Correlation and Linear Interpolation

It is noted that the maximum errors between Run #6 and Run #1 were not linear. Hence, at least three error maps, such as at Run #6, Run #3, and Run #1, are needed to get a better interpolation over the temperature range. A new error map can be generated at any thermal state by linear interpolation between two maps. Based on the correlation calculation, for linear displacement errors, use the temperature measured at *x*-middle (same as the *y*-front) for $D_x(x)$, and $D_y(y)$; use the temperature at *z*-column for $D_z(z)$. For squareness errors, use the temperature measured at *x*-middle for *xy*-plane; use the temperature at *z*-column for *yz*-plane and *zx*-plane. For straightness errors, use the temperature measured at *x*-middle for $D_y(x)$, $D_z(x)$, $D_x(y)$, and $D_z(y)$; and the temperature at *z*-column for $D_x(z)$ and $D_y(z)$. Using three error maps and the correlated temperatures for linear interpolation, the position errors can be reduced considerably.

It is concluded that large machine temperature changes caused somewhat small straightness error changes but large squareness error changes. Using the measured position errors, several error maps could be generated. Compensation tables at an actual thermal state can be interpolated to achieve higher accuracy at various thermal loadings.

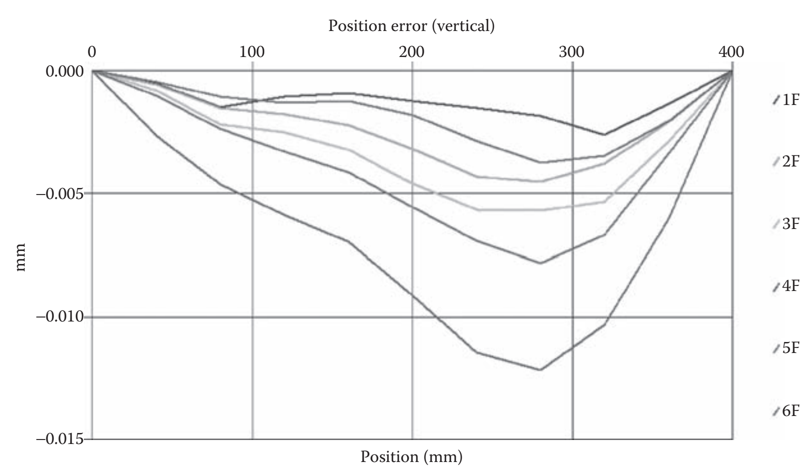

FIGURE 8.9 (See color insert following page XXX.) Measured *y*-axis straightness errors *Dx*(*y*) at six different thermal conditions, Run #1 to Run #6.

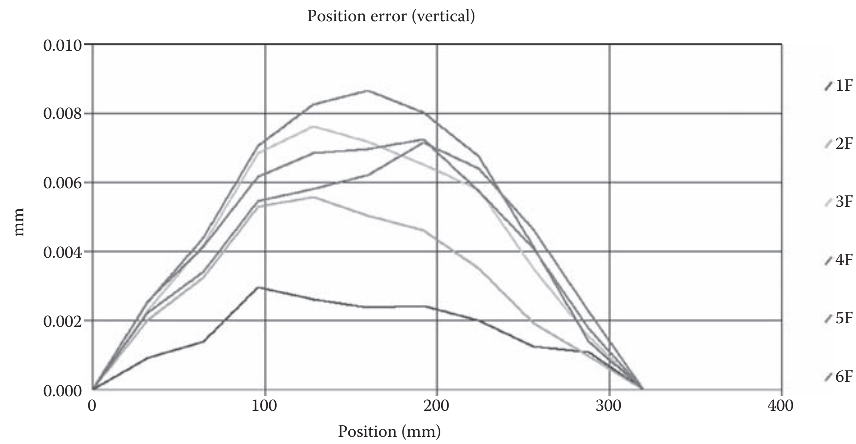

FIGURE 8.10 (See color insert following page XXX.) Measured z-axis straightness errors $Dx(z)$ at six different thermal conditions, Run #1 to Run #6.

8.3 POSITIONING ERROR MEASUREMENT USING LASER INTERFEROMETERS

Laser interferometers are becoming more popular and widely used in the machine tool industries for the calibration, compensation, and certifying machine tool positioning accuracy. Most of the laser interferometers are based on Michelson interferometer. Briefly, a laser beam is split into two beams by a beam splitter. One beam is reflected back from a fixed reference retroreflector and the other is reflected back from a target retroreflector attached to the machine's moving element. The two reflected beams are recombined by another beam splitter in front of a detector. The interference of these two beams generated a fringe pattern. When the target moves, the corresponding fringe pattern also moves. For each passing fringe, the detector will measure a cycle of high and low intensities. This one cycle corresponds to one count which is equal to a displacement of one half-wavelength. Hence, the total distance moved is equal to the half-wavelength times the number of counts.

A typical laser interferometer consists of a laser beam, remote interferometer, target retroreflector, photodetector, and electronics. For a conventional laser interferometer, the exit laser beam and the return laser beam are parallel but displaced by about 1 in., as shown in Figure 8.11. The laser Doppler displacement meter (LDDM™) is a two-frequency AC interferometer [10]. It uses a single-aperture optical arrangement, the output laser beam, and the return laser beam passing through the same aperture as shown in Figure 8.11. Hence, a small retroreflector or a flat mirror can be used as target. Therefore, the laser system becomes very compact and versatile.

8.3.1 Direct Measurement of Positioning Errors

Using a conventional laser interferometer, the linear displacement errors and angular errors can easily be measured. However, the straightness error and the squareness errors are very difficult to measure. This is because very complex and expensive optics, such as Wollaston prism, are used. With the complex optics, it is very difficult to set up and align. It usually takes days of machine downtime and experienced operator to perform these measurements. Hence, the measurement of 21 rigid-body errors is very difficult and time consuming.

8.3.2 Indirect Measurement of Positioning Errors

Direct measurement means each measurement is independent and the difference between measured position and the targeted position is the positioning error. Indirect measurement means several measurements are required to determine the final positioning errors, and the measurement error is limited by the repeatability of the machine. Based on this concept and also the concept that the measurement

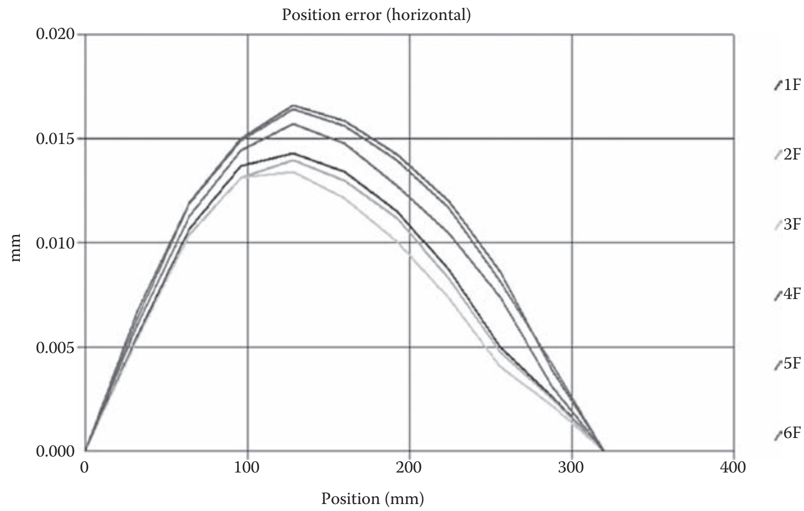

FIGURE 8.11 Measured z-axis straightness errors $Dy(z)$ at six different thermal conditions, Run #1 to Run #6.

direction is not parallel to the movement direction, Optodyne has developed a laser vector technique for the measurement of 3D volumetric positioning errors, including three linear displacement errors, six straightness errors, and three squareness errors in a very short time [13,14].

8.3.2.1 Body Diagonal Displacement Measurement

Using a conventional laser interferometer to measure the straightness and squareness errors is rather difficult and costly. It usually takes days of machine downtime and experienced operator to perform these measurements. For these reasons, the body diagonal displacement error defined in the ASME B5.54 or ISO 230-6 standard is a good quick check of the volumetric error [11,12]. Furthermore, it has been used by Boeing Aircraft Company and many others for many years with very good results and success.

Briefly, similar to a laser linear displacement measurement, instead of pointing the laser beam in the axis direction, pointing the laser beam in the body diagonal direction as shown in Figure 8.12.

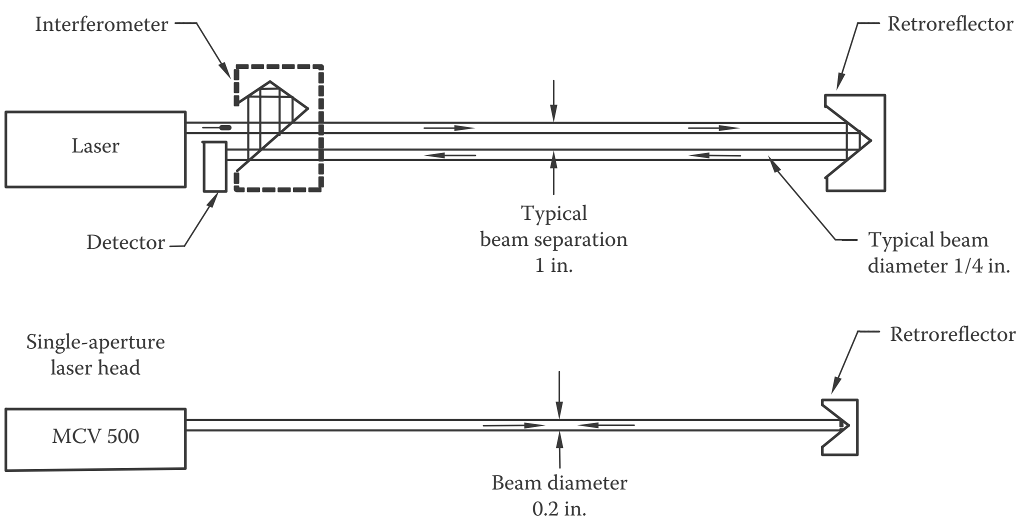

FIGURE 8.12 A comparison of a laser interferometer and a single-aperture laser Doppler system.

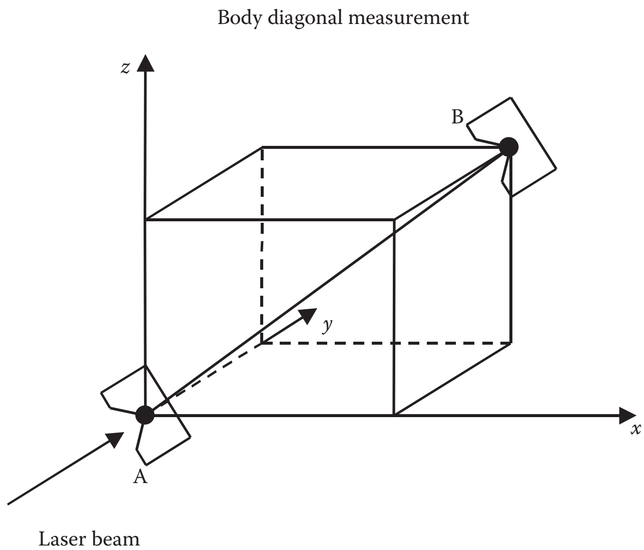

FIGURE 8.13 The body diagonal displacement measurement.

Mount a retroreflector on the spindle and move the spindle in the body diagonal direction. Starting from the zero position and at each increment of the three axes, which are moved together to reach the new position along the diagonal, the displacement error is measured. There are four body diagonal directions as shown in Figure 8.13. The accuracy of each position along the diagonal depends on the positioning accuracy of the three axes, including the straightness errors, angular errors, and squareness errors. Hence, the four body diagonal displacement measurements are a good method for the machine verification.

The relations between the measured four body diagonal displacement errors and the 21 rigid-body errors can be derived by the formulae in Section 1.3.3. For the *FXYZ*, the measured error DR at each increment can be expressed as [5,6]

$$\begin{aligned}\mathrm{DR}_{\mathrm{ppp}} = {} & a/r * D_x(x) + b/r * D_y(x) + c/r * D_z(x) + a/r * [D_x(y) + yS_{xy}] \\ & + b/r * D_y(y) + c/r * D_z(y) + a/r * [D_x(z) + z\,S_{zx}] \\ & + b/r * [D_y(z) + z\,S_{yz}] + c/r * D_z(z) + A_y(x) * ac/r \\ & - A_z(x) * ab/r + A_y(y) * ac/r - A_x(y) * bc/r\end{aligned} \tag{8.108}$$

$$\begin{aligned}\mathrm{DR}_{\mathrm{npp}} = {} & -a/r * D_x(x) + b/r * D_y(x) + c/r * D_z(x) - a/r * [D_x(y) + y\ S_{xy}] \\ & + b/r * D_y(y) + c/r * D_z(y) - a/r * [D_x(z) + z\ S_{zx}] \\ & + b/r * [D_y(z) + z\ S_{yz}] + c/r * D_z(z) - A_y(x) * ac/r \\ & + A_z(\mathrm{x}) * ab/r - A_y(\mathrm{y}) * ac/r - A_x(y) * bc/r\end{aligned} \tag{8.109}$$ AQ8

$$\begin{aligned}\mathrm{DR}_{\mathrm{pnp}} = {} & a/r * D_x(x) - b/r * D_y(x) + c/r * D_z(x) + a/r * [D_x(y) + yS_{xy}] \\ & - b/r * D_y(y) + c/r * D_z(y) + a/r * [D_x(z) + z\ S_{zx}] \\ & - b/r * [D_y(z) + z\ S_{yz}] + c/r * D_z(z) + A_y(x) * ac/r \\ & + A_z(x) * ab/r + A_y(y) * ac/r + A_x(y) * bc/r\end{aligned} \tag{8.110}$$

$$
\begin{aligned}
\mathrm{DR}_{\mathrm{ppn}} = {} & a/r * D_x(x) + b/r * D_y(x) - c/r * D_z(x) + a/r * [D_x(y) + y\ S_{xy}] \\
& + b/r * D_y(y) - c/r * D_z(y) + a/r * [D_x(z) + z\ S_{zx}] \\
& + b/r * [D_y(z) + z\ S_{yz}] - c/r * D_z(z) - A_y(x) * ac/r \\
& - A_z(x) * ab/r - A_y(y) * ac/r + A_x(y) * bc/r
\end{aligned} \tag{8.111}
$$

where the subscript ppp means body diagonal with all x, y, and z positive; npp means body diagonal with x negative, y and z positive; pnp means body diagonal with y negative, x and z positive; and ppn means body diagonal with z negative, x and y positive. Also a, b, c, and r are increments in x, y, z, and body diagonal directions, respectively. The body diagonal distance can be expressed as $r^2 = a^2 + b^2 + c^2$.

In the *FXYZ* configuration shown in Equations 8.108 through 8.112, there are four angular error terms, $A_y(x)^* ac/r$, $-A_z(x)^* ab/r$, $A_y(y)^* ac/r$, and $-A_x(y)^* bc/r$. In the *XFYZ* configuration, most of the angular error terms are cancelled and only two angular error terms, $A_y(y)^* ac/r$ and $-A_x(y)^* bc/r$, are left. Similarly, in the *XYFZ* configuration, only two angular error terms, $A_z(x)^* ab/r$ and $-A_x(x)^* bc/r$, are left. Finally, in the *XYZF* configuration, there are four angular error terms, $A_y(x)^* ac/r$, $-A_z(x)^* ab/r$, $A_y(y)^* ac/r$, and $-A_x(y)^* bc/r$ exactly the same as in the *FXYZ* configuration. Since the configurations for most common horizontal machining centers and vertical machining centers are *XFYZ* and *XYFZ*, respectively, we can conclude that the body diagonal displacement measurement is not sensitive to angular errors. AQ9

It is noted that if the four body diagonal displacement errors are small, then the machine errors are most likely very small. If the four body diagonal displacement errors are large, then the machine errors are large. However, because there are only four sets of data and there are nine sets of errors, we do not have enough information to determine which errors are large. In order to determine where the large errors are, the sequential step diagonal measurement or laser vector technique [13,14] has been developed by Optodyne to collect 12 sets of data with the same four diagonal setups. Based on these data, all three displacement errors, six straightness errors, and three squareness errors can be determined. Furthermore, the measured positioning errors can also be used to generate a 3D volumetric compensation table to correct the positioning errors and achieve higher positioning accuracy. Hence, 3D volumetric positioning errors can be measured without incurring high costs and long machine tool downtime.

The four body diagonal displacement errors shown in Equations 8.108 through 8.112 are sensitive to all of the nine linear errors and some angular errors. Hence, it is a good measurement of the 3D volumetric positioning errors. The errors in the above equations may be positive or negative and they may cancel each other. However, the errors are statistical in nature, the probability that all of the errors will be cancelled in all of the positions and in all of the four body diagonals are theoretically possible but very unlikely. Hence, it is indeed a quick measurement of volumetric positioning accuracy. AQ10

8.3.2.2 Vector or Sequential Step Diagonal Displacement Measurement

To overcome the limitations in the four body diagonal displacement measurement, a sequential step diagonal or vector technique [13–16] has been developed by Optodyne. The basic concept of the vector method is that the laser beam direction (or the measurement direction) is not parallel to the motion of the linear axis. Hence, the measured displacement errors are sensitive to the errors both parallel and perpendicular to the direction of the linear axis. More precisely, the measured linear errors are the vector sum of errors, namely, the displacement errors (parallel to the linear axis), the vertical straightness errors (perpendicular to the linear axis), and horizontal straightness errors (perpendicular to the linear axis and the vertical straightness error direction), projected to the direction of the laser beam. Furthermore, collect data with the laser beam pointing in three different diagonal directions; all nine error components can be determined. Since the errors of each axis of motion are the vector sum of the three perpendicular error components, we call this measurement a "vector" method.

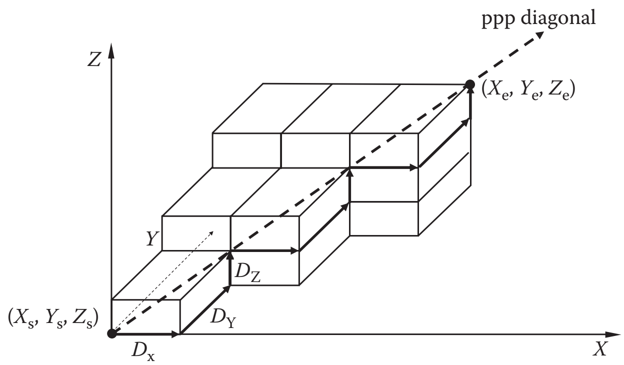

FIGURE 8.14 Vector measurement trajectory, the laser is pointing in the ppp diagonal Direction. Move *Dx*, stop, collect data; move *Dy*, stop; and move *Dz*, stop, collect data, and so on.

For conventional body diagonal displacement measurement, all three axes move simultaneously, the displacement is a straight line along the body diagonal; hence, a laser interferometer can be used to do the measurement. However, for the vector measurement described here, the displacements are along the *x*-axis, *y*-axis, and *z*-axis. The trajectory of the target or the retroreflector is not parallel to the diagonal direction as shown in Figure 8.14. The deviations from the body diagonal are proportional to the size of the increment *X*, *Y*, or *Z*. A conventional laser interferometer will be a way-out of alignment even with an increment of a few millimeter.

To tolerate such large lateral deviations, an LDDM using a single-aperture laser head and a flat mirror as the target can be used [10]. This is because any lateral movement or movement perpendicular to the normal direction of the flat mirror will not displace the laser beam. Hence, the alignment is maintained. After three movements, the flat-mirror target will move back to the center of the diagonal again; hence, the size of the flat mirror has only to be larger than the largest increment. A schematic showing the flat-mirror positions during the measurement steps is shown in Figure 8.15. Here, the flat-mirror target is mounted on the machine spindle and it is perpendicular to the laser beam direction.

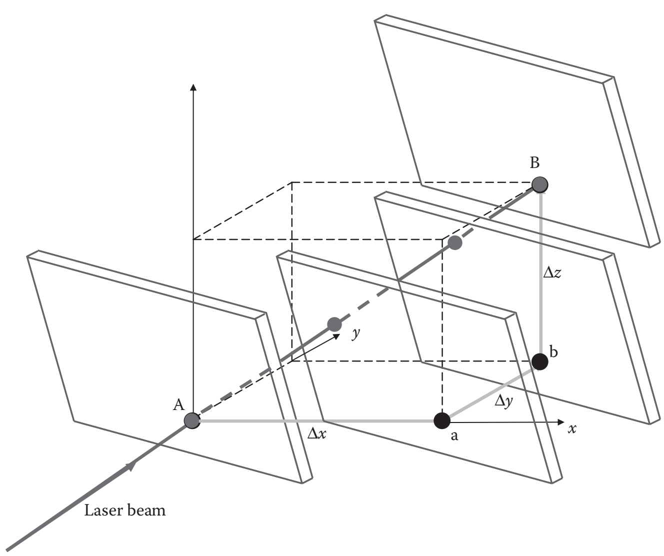

FIGURE 8.15 (See color insert following page XXX.) Sequential step diagonal or vector technique.

For this reason, three times more data is collected and also the positioning error due to each single axis movement can be separated. The collected data can be processed as the projection of the displacement of each single axis along the diagonal. In summary, in a conventional body diagonal measurement all three axes move simultaneously along a body diagonal and collect data at each preset increment. In the vector measurement all three axes move in sequence along a body diagonal and collect data after each axis is moved. Hence, not only three times more data are collected, the error due to the movement of each axis can also be separated.

In practice, first, point the laser beam in one of the body diagonal directions, similar to the body diagonal displacement measurement in the ASME B5.54 standard. However, instead of programing the machine to move, x, y, and z continuously to the next increment, stop and take a measurement, the machine is now programed to, move the x-axis, stop and take a measurement, then move the y-axis, stop and take a measurement, then move the z-axis, stop and take a measurement. A typical setup on a CNC machining center is shown in Figure 8.16.

As compared to the conventional body diagonal measurement where only one data point is collected at each increment in the diagonal direction, the vector measurement collects three data points, one after x-axis movement, one after y-axis movement, and one after z-axis movement. Hence, three times more data is collected.

Second, point the laser beam in another body diagonal direction and repeat the same until all four body diagonals are measured. Since each body diagonal measurement collected three sets of data, there are 12 sets of data. Hence, there are enough data to solve the three displacement errors, six straightness errors, and the three squareness errors. The setup is simple and easy and the measurement can be performed in a few hours instead of a few days using a conventional laser interferometer.

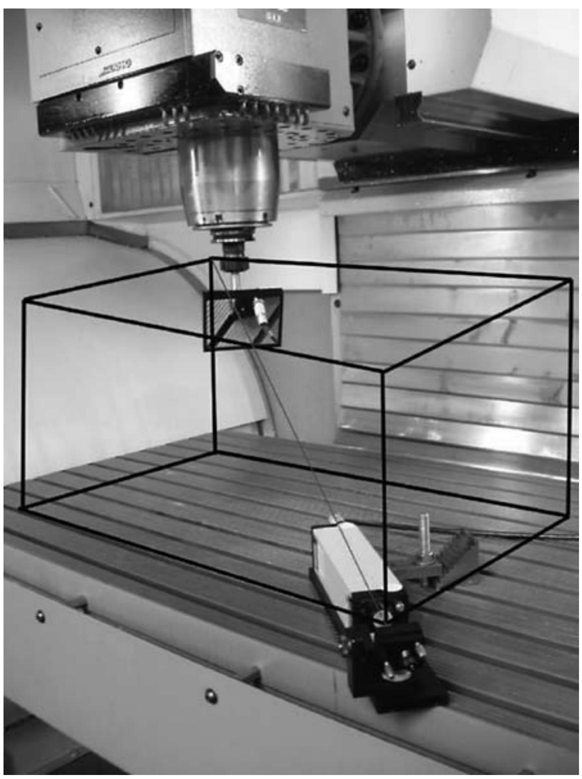

FIGURE 8.16 (See color insert following page XXX.) A photo of actual laser setup for the vector measurement.

8.4 APPLICATIONS

Many machine tool controllers can provide volumetric positioning error compensations for repeatable linear position and straightness errors on each linear axis of motion. For most controllers, there are compensations for linear errors (or pitch errors) and straightness error (or cross errors, droop errors, sag errors, nonlinear errors).

8.4.1 Siemens Controller—Sag Compensation

The Siemens 840 controllers has 18 tables for linear and sag compensations. For each axis, there are displacement error forward, displacement error backward, horizontal straightness forward, horizontal straightness backward, vertical straightness forward, and horizontal straightness backward, a total of six tables for each axis and a total of 18 tables for three axes. A sample compensation file is shown in Table 8.3. AQ11

8.4.2 Fanuc Controller—Pitch Errors and Straightness Errors Compensation

The Fanuc 30i/31i/32i controller with 128-point option has nine compensation tables. The first three tables are for displacement errors (or pitch errors), for x-axis (DXX), y-axis (DYY), and z-axis (DZZ). The next six tables are for straightness errors, moving axis = X, compensation axis = $Y(DXY)$; moving axis = Y, compensation axis = $X(DYX)$; moving axis = Z, compensation axis = $X(DZX)$; and moving axis = Z, compensation axis = $Y(DZY)$, moving axis = X, compensation axis = $Z(DXZ)$; and moving axis = Y, compensation axis = $Z(DYZ)$. For all nine tables, the unit, the comp unit, the comp algorithm, comp digits, and travel direction should all be the same. The increment and the reference should be the same for x-, y-, and z-axes. A typical compensation file is shown in Table 8.4.

8.4.3 Heidenhain Controller—Nonlinear Compensation

The Heidenhain controller can compensate linear pitch error and volumetric positioning error (called by Heidenhain as nonlinear error compensation). The volumetric compensation has three tables for linear displacement error (pitch error) compensation and six tables for the straightness error (nonlinear error) compensation. These are $Dx(X)$, $Dy(X)$, $Dz(X)$, $Dx(Y)$, $Dy(Y)$, $Dz(Y)$, $Dx(Z)$, $Dy(Z)$, and $Dz(Z)$. A configuration file with the same name but with an extension.cma will be generated. A typical configuration file and comp file are shown in Table 8.5. AQ12

8.4.4 MDSI Controller—Position Compensation

MDSI controller is a software-based open system CNC machine tool controller that meets the CNC machine control needs of small and large manufacturers in all industries. It does not use proprietary hardware and possesses the standards required for true open-architecture controls as established by OMAC (open modular architecture controls) and OSACA (open system architecture for controls within automation systems). It allows the integration of commercial off-the-shelf hardware and software components. It was built with components found in the open market, clearly defined and published in form of specification. An open application programing interface (API) is available in the MDSI open controller for customer to integrate third party application. The controller is user installable, configurable, and maintainable.

MDSI has been designed to be programmable at low level to achieve tool and fixtures offset compensation and leadscrew error compensation (LSEC). LSEC feature allows precise measurements along each axis. The deviation from the expected value due to irregularities in the leadscrew can then be compensated for. This could be done by entering variables that correspond to the measured deviations into the tune file that tell OpenCNC how to compensate the errors.

TABLE 8.3 AQ13

```
%_N_NC_CEC_INI
CHANDATA(1)
$AN_CEC[0,0]=0.0000
$AN_CEC[0,1]=+0.0001
$AN_CEC[0,2]=+0.0000
$AN_CEC[0,3]=+0.0005
$AN_CEC[0,4]=+0.0024
$AN_CEC[0,5]=+0.0036
..........................................................
..........................................................
..........................................................
$AN_CEC[0,37]=−0.0019
$AN_CEC[0,38]=−0.0016
$AN_CEC[0,39]=−0.0025
$AN_CEC[0,40]=−0.0037
$AN_CEC_INPUT_AXIS[0]=(AX1)
$AN_CEC_OUTPUT_AXIS[0]=(AX1)
$AN_CEC_STEP[0]=+50.0000
$AN_CEC_MIN[0]=−2100.0000
$AN_CEC_MAX[0]=−100.0000
$AN_CEC_DIRECTION[0]=1
$AN_CEC_MULT_BY_TABLE[0]=0
$AN_CEC_IS_MODULO[0]=0
$AN_CEC[17,0]=+0.0001
$AN_CEC[17,1]=+0.0005
$AN_CEC[17,2]=+0.0007
$AN_CEC[17,3]=−0.0015
$AN_CEC[17,4]=−0.0010
......................................................................
................................................................................
................................................................................
$AN_CEC[23,40]=−0.0085
$AN_CEC_INPUT_AXIS[23]=(AX3)
$AN_CEC_OUTPUT_AXIS[23]=(AX10)
$AN_CEC_STEP[23]=+25.0000
$AN_CEC_MIN[23]=−1125.0000
$AN_CEC_MAX[23]=−125.0000
$AN_CEC_DIRECTION[23]=−1
$AN_CEC_MULT_BY_TABLE[23]=0
$AN_CEC_IS_MODULO[23]=0
M23
```

8.4.4.1 Offline Error Compensation in MDSI

An understanding of the LSEC system can be applied in the MDSI at higher level to achieve geometric error compensation. A sample implementation of the geometric error compensation system using the LSEC approach is discussed here. Compensation data required for the LSEC system is saved in the parameter file called "Tune file" which is read by OpenCNC when the controller starts up. This file has specific format comprising variables names with values as shown in Table 8.6.

TABLE 8.4

```
%
N3620Q1A1P6A2P100A3P200
N3621Q1A1P0A2P100A3P200
N3622Q1A1P6A2P106A3P206
N3623Q1A1P1A2P1A3P1
N3624Q1A1P6000A2P3000A3P3000
N5711Q1P1
N5712Q1P2
N5713Q1P2
N5714Q1P3
N5715Q1P3
N5716Q1P1
N5721Q1P2
N5722Q1P1
N5723Q1P3
N5724Q1P1
N5725Q1P2
N5726Q1P3
N13381Q1P300
N13382Q1P400
N13383Q1P500
N13384Q1P600
N13385Q1P700
N13386Q1P800
N13391Q1P1
N13392Q1P1
N13393Q1P1
N13394Q1P1
N13395Q1P1
N13396Q1P1
%
Comp Value
%
N10000P1
N10001P0
N10002P0
N10003P0
N10004P1
N10005P0
N10006P0
N10100P0
N10101P0
N10102P0
N10103P1
..........
..........
..........
N10805P0
N10806P0
%
```

TABLE 8.5

BEGIN	CompHeidenhainConfig.CMA	ACT:0	
NR	1	2	3
0	CompHeidenhainX	CompHeidenhainY	CompHeidenhainZ
[END]			
BEGIN	CompHeidenhainX.com	DATUM: +0.0	DIST: 13
NR	1=f( )		
0	+0.0	+0	
1	+0.8192	−0.00027	
2	+1.6384	−0.00036	
3	+2.4576	−0.00036	
4	+3.2768	−0.00034	
5	+4.096	−0.00036	
6	+4.9152	−0.0004	

These are applied to existing axes of the machine tool and referred to from zero to *n* with an increment of one for each new axis. For Takisawa CNC machine* *x*, *y*, and *z* are assigned, respectively, 0,1, and 2. The arrays are described as follows:

TABLE 8.6

```
# Compensation tune file for X
 stage
#
axLSCompCount[0] 11
axLSCompSpacing[0] 5000000
axLSCompPosMin[0] 0
#
axLSCompDirNeg [0] [0]          544
axLSCompDirNeg[1][0]            230
axLSCompDirNeg[2][0]            107
axLSCompDirNeg[3][0]           −63
axLSCompDirNeg[4][0]           −309
axLSCompDirNeg[5][0]           −578
axLSCompDirNeg[6][0]           −812
axLSCompDirNeg[7][0]           −997
axLSCompDirNeg[8][0]           −1161
axLSCompDirNeg[9][0]           −1332
axLSCompDirNeg[10][0]          −1457
#
axLSCompDirPos[0] [0]           28
axLSCompDirPos[1] [0]          −28
axLSCompDirPos[2][0]           −125
axLSCompDirPos[3][0]           −304
axLSCompDirPos[4][0]           −558
axLSCompDirPos[5][0]           −858
axLSCompDirPos[6][0]           −1174
axLSCompDirPos[7][0]           −1487
axLSCompDirPos[8][0]           −1808
axLSCompDirPos[9][0]           −2188
axLSCompDirPos[10][0]          −2720
#
#
```

- axLSCompDirPos and axLSCompDirNeg: Two arrays for the direction of the movement representing LSEC data; the first dimension subscript references the compensation data points and the second references the axis number.
- axLSCompCount: The number of measured axis positions for each axis.
- axLSCompSpacing: The spacing increment between measured axis positions; axLS CompSpacing[0] comprises the distance between measurement points for axis 0 and axLSCompSpacing [l] for axis 1.
- axLSCompPosMin: The starting locations of the measured axis positions.

By convention, the starting location of the measurements is always at the most negative axis location. Each of these arrays uses the subscript to designate the machine axis the data applies to. A MATLAB program has been written to convert measurement into OpenCNC format. The Tune file is then generated and ready to be stored for the controller start-up. It is worth noting that this file is read once and kept independent from the system files to avoid any confusion.

As the axes are moved under program control, the current axis positions and directions of motion are obtained and used to determine the corresponding locations within the appropriate error arrays. The values from the arrays are used in the error equations to calculate the amounts to move each of the axes, and the modified position command is sent to the motor amplifiers. The flow diagram for obtaining the modified position command is in Table 8.7.

These steps must occur during each system interrupt. The volumetric error components are complex equations which require a corresponding CPU time to estimate the interrupt range that could be supported.

8.4.4.2 Real-Time Error Compensation

The robust and fully documented API available in MDSI OpenCNC could be used to facilitate and implement real-time error compensation and in-process gauging. This is because it provides the capability to integrate other software products or technologies as programers can write hard real-time programs using Microsoft Visual Basic.

TABLE 8.7

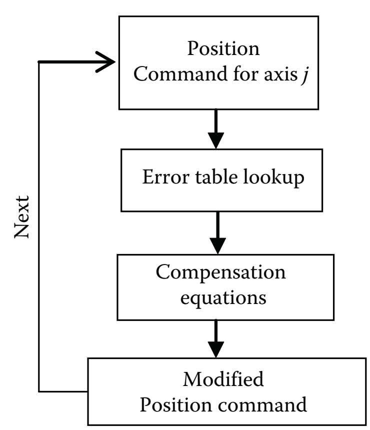

* Programme developed at the University of Manchester.

8.4.5 Other Controllers—Cross Compensation

The Fagor 8055 controller has three tables for linear displacement error (pitch error) compensation and three tables for the straightness error compensation. These are $D_x(X)$, $D_y(Y)$, $D_z(Z)$, $D_x(Y)$, $D_x(Z)$, and $D_y(Z)$. The file format is as follows:

Filename: Filename.FGR
P15 LSCRWCOM = ON, P16 NPOINTS = _____, P8 INCHES = 0, MM (G71)
1, INCH (G70)
P31 NPCROSS = _____, P54 NPCROSS2 = _____, P57 NPCROSS3 =_____,
P32 MOVAXIS = 2, P55 MOVAXIS2 = 3, P58 MOVAXIS3 = 3,
P33 COMPAXIS = 1, P56 COMPAXIS2 = 1, P59 COMPAXIS3 = 2.
Where NPOINTS=number of linear comp points, NPCROSS=number of cross comp
points, MOVAXIS=moving axis, COMPAXIS=comp axis, $X = 1$, $Y = 2$ and $Z = 3$.

8.5 CURRENT ISSUES IN MACHINE ERRORS MODELING

The volumetric error more accurately reflects the accuracy to be expected from a machine tool than any other measurement that can be made. Hence, the volumetric error should be determined and listed on the specification sheet of every machine tool offered to industry. On the other hand, the measuring of the 21 rigid-body errors is challenging and time consuming. Hence, a definition or a method of approximating true volumetric error that correlates well to true 3D positioning error, but is less difficult to measure, is very important [1].

Traditionally, manufacturers have ensured part accuracy by linear calibration of each machine tool axis. The conventional definition of the 3D volumetric positioning error is the root mean square (RMS) of the three-axis displacement error. Twenty years ago, the dominate error is the leadscrew pitch error of three axes. This definition is adequate. However, now with better leadscrew, linear encoder, and compensation, the pitch error has bee reduced considerably. The dominate errors are the squareness errors and straightness errors. Hence, the above definition is inadequate. Furthermore, using a conventional laser interferometer to measure straightness and squareness errors can be relatively difficult and time consuming.

During the past 3 years, the industry has seen demand emerge for the "volumetric accuracy" specification on machine tools. One hurdle remains: A standard definition so that everyone measures volumetric accuracy with the same yardstick. The issue has been discussed in many standards committees, machine tool builders, and the metrology community. In general, they fall into two camps: One for a definition that would define precise volumetric accuracy for all machine tools, the other for a method, being used by Boeing and others, called "body-diagonal" measurement, which give accurate volumetric measurements for most equipment.

Beyond the 21 rigid-body errors are additional nonrigid-body errors. These consider that a machine tool is not a stationary mass. Weight shifts, which mean tool position, change ever so slightly from one end of the axis to the other. For most machines, the displacement is too small for a worthwhile measurement. But for a massive gantry machine, the error can make a small, detectable difference. To determine all rigid- and nonrigid-body errors takes 45 measurements, which can take days away from production, so it is not practical for most environments.

On the other hand, the body diagonal displacement method, while not measuring all the rigid-body errors, is very representative of 3D volumetric positioning accuracy, and certainly has more potential for production. Measuring for such errors follows the natural evolution of machine-tool technology. Like wanting a car to get better gas mileage and drive faster, industry is demanding machines cut faster and more accurately at the same time. With volumetric-error compensation, manufacturers may well get just that.

8.5.1 Definitions of 3D Volumetric Error

Volumetric accuracy for movements in X, Y, Z $V(XYZ)$ is the maximum range of relative deviations between actual and ideal position in X, Y, Z and orientations in A, B, C for X, Y, Z movement in the volume concerned, where the deviations are relative deviations between the tool side and the work-piece side of the machine tool.

Assuming rigid-body motion, the formulae for the six errors in the directions of X, Y, and Z, and rotary axes A, B, and C as follows [12]:

$$\begin{aligned} V(XYZ,X) &= \text{deviations in } X \text{ at } XYZ \\ &= EXX + EXY + EXZ \end{aligned} \tag{8.112}$$

AQ14

$$\begin{aligned} V(XYZ,Y) &= \text{deviations in } Y \text{ at } XYZ \\ &= EYX + EYY + EYZ \end{aligned} \tag{8.113}$$

$$\begin{aligned} V(XYZ,Z) &= \text{deviations in } Z \text{ at } XYZ \\ &= EZX + EZY + EZZ \end{aligned} \tag{8.114}$$

$$\begin{aligned} V(XYZ,A) &= \text{angular deviations around } X \text{ at } XYZ \\ &= EAX + EAY + EAZ \end{aligned} \tag{8.115}$$

$$\begin{aligned} V(XYZ,B) &= \text{angular deviations around } Y \text{ at } XYZ \\ &= EBX + EBY + EBZ \end{aligned} \tag{8.116}$$

$$\begin{aligned} V(XYZ,C) &= \text{angular deviations around } Z \text{ at } XYZ \\ &= ECX + ECY + ECZ \end{aligned} \tag{8.117}$$

Here, the squareness errors are included in the straightness errors. The angular errors are small and can be treated as scalar.

Definition 8.1

The amplitude of the volumetric error can be defined as the RMS of the three linear deviations and the amplitude of the volumetric angular error can be defined as the RMS of the three angular deviations.

$$\begin{aligned} V(XYZ,R) = \text{SQRT}\{&V(XYZ,X)*V(XYZ,X)+V(XYZ,Y)*V(XYZ,Y) \\ &+V(XYZ,Z)*V(XYZ,Z)\} \end{aligned} \tag{8.118}$$

$$\begin{aligned} V(XYZ,W) = \text{SQRT}\{&V(XYZ,A)*V(XYZ,A)+V(XYZ,B)*V(XYZ,B) \\ &+V(XYZ,C)*V(XYZ,C)\} \end{aligned} \tag{8.119}$$

The volumetric accuracy and volumetric angular accuracy can be defined as the maximum range over the working space.

$$R_{\max} = \text{Max}\{V(XYZ,R)\} \tag{8.120}$$

$$W_{\max} = \text{Max}\{V(XYZ,W)\} \tag{8.121}$$

Definition 8.2

The maximum range of error in each direction can be expressed as

$$X_{max} = \mathrm{Max}\{V(XYZ, X)\} - \min\{V(XYZ, X)\} \tag{8.122}$$

$$Y_{max} = \mathrm{Max}\{V(XYZ, Y)\} - \min\{V(XYZ, Y)\} \tag{8.123}$$

$$Z_{max} = \mathrm{Max}\{V(XYZ, Z)\} - \min\{V(XYZ, Z)\} \tag{8.124}$$

$$A_{max} = \mathrm{Max}\{V(XYZ, A)\} - \min\{V(XYZ, A)\} \tag{8.125}$$

$$B_{max} = \mathrm{Max}\{V(XYZ, B)\} - \min\{V(XYZ, B)\} \tag{8.126}$$

$$C_{max} = \mathrm{Max}\{V(XYZ, C)\} - \min\{\mathrm{V}(XYZ, C)\} \tag{8.127}$$

The volumetric accuracy and volumetric angular accuracy can be defined as the RMS of the maximum range of error in each direction.

$$R_{max} = \mathrm{SQRT}\{X_{max} * X_{max} + Y_{max} * Y_{max} + Z_{max} * Z_{max}\} \tag{8.128}$$

$$W_{max} = \mathrm{SQRT}\{A_{max} * A_{max} + B_{max} * B_{max} + C_{max} * C_{max}\} \tag{8.129}$$

The above two equations are valid definitions. However, to determine the volumetric error, it requires extensive and time-consuming measurement. A third definition is to use the four body diagonal displacement errors to define the volumetric accuracy.

8.5.2 New Definition of 3D Volumetric Error Based on the Body Diagonal Errors

The performance or accuracy of a machine tool is determined by 3D volumetric positioning error, which includes linear displacement error, straightness error, angular error, and thermally induced error. The body diagonal displacement error defined in ASME B5.54 or ISO 230-6 is a good quick check of volumetric error. All the errors will contribute to the four body diagonal displacement errors. The B5.54 tests have been used by Boeing Aircraft Co. and others for years.

When using body diagonal displacement error measurement, body diagonal error (Ed) does not include squareness errors. But Ed is currently defined in ISO 230-6 and ASME B5.54 as a measure of volumetric error. Squareness errors can be included, and our new proposed measure volumetric error, ESd, includes squareness errors.

Some definitions: ppp/nnn indicates body diagonal direction with the increments in X, Y, and Z all positive/negative, and npp/pnn indicates the increments in X, Y, and Z are negative/positive, positive/negative, and positive/negative, etc. Body diagonal errors in each direction are Dr(r) ppp/nnn, Dr(r) npp/pnn, Dr(r) pnp/npn, and Dr(r) ppn/nnp. Based on the definition in ISO 230-6, E is defined as

$$\mathrm{E}_{ppp/nnn} = \max[\mathrm{Dr(r)ppp/nnn}] - \min[\mathrm{Dr(r)ppp/nnn}] \tag{8.130}$$

$$\mathrm{E}_{npp/pnn} = \max[\mathrm{Dr(r)npp/pnn}] - \min[\mathrm{Dr(r)npp/pnn}] \tag{8.131}$$

$$\mathrm{E}_{pnp/npn} = \max[\mathrm{Dr(r)pnp/npn}] - \min[\mathrm{Dr(r)pnp/npn}] \tag{8.132}$$

$$\mathrm{E}_{ppn/nnp} = \max[\mathrm{Dr(r)ppn/nnp}] - \min[\mathrm{Dr(r)ppn/nnp}] \tag{8.133}$$

And volumetric error is defined as

$$\mathrm{Ed} = \max[\mathrm{E}_{\mathrm{ppp/nnn}}, \mathrm{E}_{\mathrm{npp/pnn}}, \mathrm{E}_{\mathrm{pnp/npn}}, \mathrm{E}_{\mathrm{ppn/nnp}}]$$

This definition does not include squareness errors. To include squareness errors, define the volumetric error as

$$\begin{aligned}\mathrm{ESd} = &\ \mathrm{Max}[\mathrm{Dr(r)ppp/nnn}, \mathrm{Dr(r)npp/pnn}, \mathrm{Dr(r)pnp/npn}, \mathrm{Dr(r)ppn/nnp}] \\ &-\min[\mathrm{Dr(r)pp/nnn}, \mathrm{Dr(r)npp/pnn}, \mathrm{Dr(r)pnp/npn}, \mathrm{Dr(r)ppn/nnp}]\end{aligned}$$

The definition ELv is still commonly used as the definition of a 3D volumetric error, and ELSv including straightness and squareness errors is a true volumetric error. The Ed is defined in ISO 230-6 and ASME B5.54 as a measure of volumetric error. The ESd, including squareness errors, should be a good measure of volumetric error.

To demonstrate this new definition, measurements were performed on 10 selected CNC machine tools, representing the modern mid-size CNC machining centers [1]. Eight were made by the German manufacturer Deckel Maho Gildemeister (DMG), 1 by the U.K. Bridgeport, and 1 by the Czech company Kovosvit MAS. The DMG machines are for better illustration inscribed with a number behind each type description (e.g., DMU80T-2). A brief description of the 10 machines is in Table 8.1.

The measurement results are shown in Table 8.2. Measurements according to ISO 230-2 were performed along the three edges of the machine working volume. These are identified by the marks I, II, and III. The angular errors are derived from the linear positioning by respecting the Abbé offsets. The diagonal positioning accuracy is described by the parameter Ed (diagonal systematic deviation of positioning) according to ISO 230-6. The remaining geometric errors were evaluated from the laser vector method.

The 3D volumetric errors, such as ELv, ELSv, Ed, and ESd, are calculated and tabulated in Table 8.2. As compared with the true 3D volumetric error ELSv, the ELv and the ED underestimate the 3D AQ15
volumetric error, but the Ed varies with the squareness errors. The ESd also underestimates the 3D volumetric position error but relatively stable and not effected by the squareness errors.

TABLE 8.1
Machine Parameters of the 10 Selected Modern Machining Centers

Machine no.	1	2	3	4	5
Machine id.	DMC60H-1	DMC60H-2	DMC65V-1	DMC65V-2	DMU80T-1
Manufacturer	DMG	DMG	DMG	DMG	DMG
Type	Horizontal	Horizontal	Vertical	Vertical	Vertical
Axis stroke (*X*/*Y*/*Z*) mm	600/560/560	600/560/560	650/500/500	650/500/500	880/630/630
Control sys.	Sinumerik 840D	Sinumerik 840D	Sinumerik 840D	Sinumerik 840D	Heidenhein iTNC530
Service hours	2589	1655	3550	3338	2847
Machine no.	6	7	8	9	10
Machine id.	DMU80T-2	DMU80T-3	DMU80T-4	VMC500	MCV1000
Manufacturer	DMG	DMG	DMG	Bridgeport	MAS
Type	Vertical	Vertical	Vertical	Vertical	Vertical
Axis stroke (*X*/*Y*/*Z*) mm	880/630/630	880/630/630	880/630/630	650/500/500	1016/610/720
Control sys.	Heidenhein TNC430	Heidenhein iTNC530	Heidenhein TNC430	Heidenhein TNC410	Heidenhein iTNC530
Service hours	4081	1672	3723	892	437

TABLE 8.2
Measurement Results

Measurement Technique.	Error Type	Positions	Machine No.										
			1	*2*	*3*	*4*	*5*	*6*	*7*	*8*	*9*	*10*	AQ16
			Maximal deviation (μm);resp. (μm/m)										
ISO 230-2	$D_x(x)$	I	9.5	5.3	16.5	24.0	35.8	23.5	10.7	20.5	7.6	12.3	
		II	7.2	7.3	31.1	22.5	47.7	24.1	12.0	54.3	—	—	AQ17
		III	—	—	19.2	19.0	51.6	28.4	—	29.4	—	—	
ISO 230-2	$D_z(z)$	I	—	36.3	10.9	10.6	14.0	16.5	6.8	6.6	23.3	14.1	
		II	14.3	17.8	14.9	7.1	15.5	19.2	8.4	8.7	—	—	
		III	25.2	21.1	10.1	7.7	18.0	15.2	7.7	15.7	—	—	
Calc	$A_x(z)$		—	−99.0	−2.0	5.0	−5.0	−8.0	−3.0	−15.0	—	—	
	$A_y(z)$		—	−72.0	5.0	−14.0	7.0	15.0	−7.0	−6.0	—	—	
ISO 230-6	Ed		15.9	33.4	34.4	38.3	45.4	31.8	15.8	41.5	33.2	26.9	
Laser vector method	$D_x(x)$		2.7	8.4	20.2	7.8	18.6	11.8	1.7	16.8	12.8	6.9	
	$D_y(x)$		2.9	2.9	7.5	2.9	3.9	5.6	6.2	2.8	7.1	15.6	
	$D_z(x)$		2.4	3.4	9.2	4.1	2.5	3.1	2.4	1.9	8.5	6.6	
	$D_y(y)$		2.2	8.2	15.2	8.3	14.0	8.9	1.5	12.6	8.2	9.4	
	$D_z(y)$		2.3	2.8	2.3	1.2	2.0	4.0	7.3	3.3	2.3	3.5	
	$D_x(y)$		2.4	8.8	6.7	11.9	5.2	4.5	10.3	4.0	18.4	7.9	
	$D_z(z)$		2.6	9.7	10.8	4.2	10.8	6.8	2.7	9.7	15.3	7.8	
	$D_y(z)$		6.1	13.1	5.3	23.3	25.1	23.9	5.2	9.3	27.5	21.3	
	$D_x(z)$		15.9	28.2	7.2	5.2	5.2	2.1	8.5	15.8	25.6	6.4	
	Bxy		−1	15	−18	−8	5	3	15	−8	56	11	
	Bxz		41	−52	−31	−7	7	4	−18	−39	64	−37	
	Byz		−18	−18	−8	−67	−53	−48	−16	−27	73	−7	
3D Volumetric errors	ESd		30	33	33	33	46	34	27	45	54	44	
	ELv		25.55	27.13	27.62	31.61	51.95	35.59	20.18	39.61	28.03	24.43	
	ELSv		42.81	58.66	49.31	62.89	77.05	62.37	43.56	62.58	78.41	63.72	
	Ed		15.9	33.4	34.4	38.3	45.4	31.8	15.8	41.5	33.2	26.9	
	ELSv/ELv		1.67	2.16	1.79	1.99	1.48	1.75	2.16	1.58	2.80	2.61	
	ELSv/Ed		2.69	1.76	1.43	1.64	1.70	1.96	2.76	1.51	2.36	2.37	
	ELSv/ESd		1.43	1.78	1.49	1.91	1.67	1.83	1.61	1.39	1.45	1.45	
Calc	$A_y(x)$		—	—	53.0	4.0	−12.0	−7.0	—	14.0	—	—	
	$A_z(x)$		—	—	15.0	26.0	−36.0	5.0	—	84.0	—	—	
ISO 230-2	$D_y(y)$	I	15.8	7.8	15.3	18.4	20.3	14.3	16.2	5.5	13.6	15.7	
		II	12.0	8.7	4.9	20.4	18.3	19.2	17.1	6.3	—	—	
		III	—	—	13.2	24.9	22.9	21.6	11.2	12.1	—	—	
Calc	$A_x(y)$		—	—	60.0	−12.0	11.0	−3.0	7.0	−8.0	—	—	
	$A_z(y)$		—	—	38.0	6.0	2.0	−3.0	−9.0	28.0	—	—	

For more quantitative comparison, a multiple factor, M1, is defined as ELSv/ELv, M2 as ELSv/Ed, and M3 as ELSv/ESd. Hence, the true 3D volumetric error ELSv can be obtained by multipling the ELv by M1, the Ed by M2, and the ESd by M3. The multiple factors M1, M2, and M3 for various

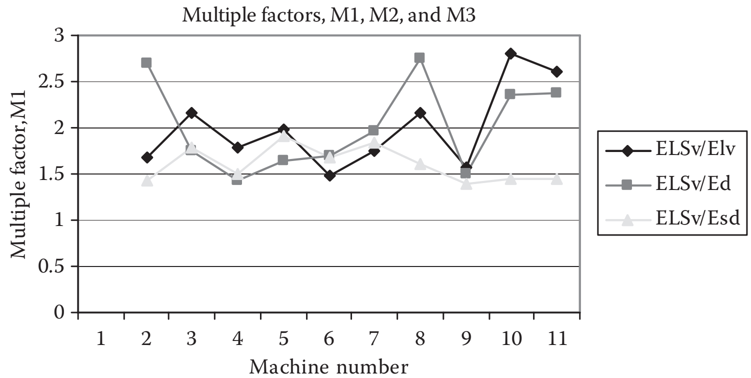

FIGURE 8.17 Multiple factors for various definitions of volumetric errors.

machine tools are plotted in Figure 8.17. The M1 varies from 1.4 to 2.8, the M2 from 1.43 to 2.76, and the M3 from 1.4 to 1.9. The range of variations for M1 and M2 are relatively large, while it is relatively small for M3. Hence, the ESd is a good estimate of 3D volumetric position error.

8.6 SUMMARY AND CONCLUSION

Four definitions of the 3D volumetric positioning error have been provided. The positioning errors of 10 CNC machine tools have been measured. Based on these measurement results, the 3D volumetric errors using various definitions can be calculated. It is concluded that the laser body diagonal displacement measurement in the ASME B5.54 or ISO 230-6 machine tool performance measurement standards is a quick check of the volumetric positioning error and the value ESd is a good measure of the volumetric error.

Measurements performed on 10 mid-size machining centers reveal that when compared to true 3D volumetric error ELSv, ELv underestimates volumetric error. The Ed underestimates true volumetric error and varies with squareness errors. Finally, ESd underestimates 3D volumetric position error but is relatively stable and not influenced by squareness errors. Thus ESd is a good measure of volumetric error.

REFERENCES

1. C. Wang, O. Svoboda, P. Bach, and G. Liotto, Definitions and correlations of 3D volumetric positioning errors of CNC machining centers, *Proceedings of the IMTS 2004 Manufacturing Conference*, Chicago, IL, September 8–10, 2004.
2. R. Schultschik, The components of the volumetric accuracy, *Annals of the CIRP*, 25(1), 223–228, 1977.
3. W. Beckwith Jr. and R.I. Warwick, Method for calibration of coordinate measuring machine, US Patent 4,939,678, July 3, 1990.
4. G. Zhang, R. Quang, B. Lu, R. Hocken, R. Veale, and A. Donmez, A displacement method for machine geometry calibration, *CIRP*, 37(1), 515–518, 1988.
5. G. Ren, J. Yang, G. Liotto, and C. Wang, Theoretical derivations of 4 body diagonal displacement errors in 4 machine configurations, *Proceedings of the LAMDAMAP Conference,* Cransfield, UK, June 27–30, 2005.
6. C. Wang and G. Liotto, A theoretical analysis of 4 body diagonal displacement measurement and sequential step diagonal measurement, *Proceedings of the LAMDAMAP 2003*, Huddersfield, England, July 1–4, 2003.
7. *Fanuc 3D Grid Point Compensation Manual*, 2003. AQ18
8. O. Svoboda, P. Bach, G. Liotto, and C. Wang, Machine tool 3D volumetric positioning error measurement under various thermal conditions, *Proceedings of the ISPMM 2006 Conference*, Urumqi, Xinjiang, China, August 2–6, 2006.

9. O. Svoboda, P Bach, J. Yang, and C. Wang, Correlation of 3D volumetric positioning errors and temperature distributions - Theory and measurement, *Proceedings of the ISICT 2006 Conference,* Beijing, China, October 13-15, 2006.
10. C. Wang, Laser Doppler displacement measurement, *Lasers and Optronics,* 6, 69 - 71, 1987.
11. *Methods for Performance Evaluation of Computer Numerically Controlled Machining Centers, An American National Standard,* ASME B5.54-1992 by the American Society of Mechanical Engineers, p. 69, 1992. AQ19
12. ISO 230-6: 2002 Test code for machine tools - Part 6: Determination of positioning accuracy on body and face diagonals (diagonal displacement tests), *An International Standard,* by International Standards Organization, 2002.
13. C. Wang, Laser vector measurement technique for the determination and compensation of volumetric positioning errors. Part I: Basic theory, *Review of Scientific Instruments,* 71(10), 3933-3937, 2000.
14. J. Janeczko, R. Griffin, and C. Wang, Laser vector measurement technique for the determination and compensation of volumetric position errors, Part 11: Experimental verification, *Review of Scientific Instruments,* 71, 3938-3941, 2000.
15. O. Svoboda, P Bach, G. Liotto, and C. Wang, Volumetric positioning accuracy: Measurement, compensation and verification, *Proceedings of the JUSFA 2004 Conference,* Denver, CO, July 19-21, 2004.
16. O. Svoboda, Milling machine tools' accuracy in thermally unbalanced conditions, Ph.D. Thesis, Czech Technical University in Prague, July 2007.